Characterization of the interfacial properties of compound-extruded lightweight profiles using the push-out-technique

Kay A. Weidenmann, E. Kerscher, V. Schulze, D. Löhe

Angaben zur Veröffentlichung / Publication details:

Weidenmann, Kay A., E. Kerscher, V. Schulze, and D. Löhe. 2006. "Characterization of the interfacial properties of compound-extruded lightweight profiles using the push-out-technique." *Materials Science and Engineering: A* 424 (1-2): 205–11. https://doi.org/10.1016/j.msea.2006.03.038.

Characterization of the interfacial properties of compound-extruded lightweight profiles using the push-out-technique

K.A. Weidenmann *, E. Kerscher, V. Schulze, D. Löhe

Institut für Werkstoffkunde I, Universität Karlsruhe (TH), Karlsruhe, Germany

1. Introduction

Aluminium and its alloys are highly qualified candidate materials for automotive lightweight constructions due to their low density in addition to outstanding formability. If the designed space is limited, reinforced aluminium-matrix-based profiles present an attractive solution to increase both specific stiffness and specific strength. The bar extrusion technology represents a promising alternative to conventional casting techniques and is a solid state manufacturing route for composites. This can be realized in two different ways: first, the regular extrusion of discontinuously reinforced composite billets or, secondly, the compound extrusion of regular billets using modified extrusion dies which allow for an in situ continuous reinforcement during the extrusion process. In the welding chamber of the extrusion press, the reinforcing elements, e.g. wires or ropes, are embedded into the matrix under high pressure at high temperature with controlled position inside the profile to optimize the load capacity [1].

* Corresponding author. Tel.: +49 721 608 4165; fax: +49 721 608 8044.
E-mail address: kay.weidenmann@iwk1.uni-karlsruhe.de
(K.A. Weidenmann).

The internal load transfer between matrix and reinforcing element is a crucial factor for the composite's performance. Therefore, the investigation methods to be used should allow for a quantitative evaluation of the fibre-matrix debonding shear strength as well as for receiving a qualitative impression of the interface. The debonding shear strength in aluminium–steel compound conductor rails has already been determined, admittedly with both of the compound partners lying on the surface. For this compound the AA6060 in the artificially aged state T6, the debonding shear strength reached 100 MPa [2]. For the reinforcing element completely surrounded by matrix material the single fibre push-out-test is a method approved for measuring the debonding shear strength as proposed by Marshall [3]. A single reinforcing element is loaded by applying an indenter or plunger until the interface fails and the element is pushed out continuously. Ideally, this impact is considered as pure shear load. In fact, the transversal expansion of the reinforcing element induces a compressive stress on the interface [4]. Disregarding this stress, the debonding shear strength can be calculated from the maximum axial load (see Fig. 1) by using Eq. (1):

$$\tau_{\max} = \frac{F_{\max}}{\pi d h}, \tag{1}$$

where the diameter of the fibre d and the sample thickness h are assumed [5,6]. Push-out-tests on fibre-reinforced com-

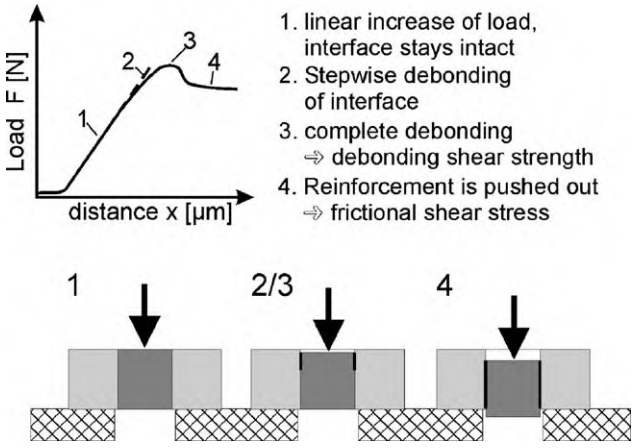

Fig. 1. Functional principle and schematic load–displacement-graph of a fibre push-out-test [5].

posites are well-established when focussing on ceramic fibres [3,6].

2. Experimental

2.1. Sample materials

The profiles having a rectangular cross-section of 56 mm × 5 mm were compound-extruded on a 10 MN-extrusion press, fan-cooled and naturally aged (heat treatment T4). The profiles have an AA6060-matrix, which was reinforced with wires with a diameter of 1 mm made from the stainless spring steel 1.4310, cobalt-base alloy Haynes 25 or nickel-base alloy Inconel 718. The two last-mentioned alloys with an excellent high temperature resistance withstand the thermal impact during the extrusion process more easily than stainless spring steels do. Furthermore, for the binary systems nickel–aluminium and cobalt–aluminium, the formation of strength-enhancing intermetallic phases is predicted [7]. The reinforcing wires have been cleaned with acetone prior to the extrusion process (initial state). Additionally, some wires have been ground, pickled with stainless steel pickle or sandblasted before they were incorporated into the matrix material. Some profiles were solution annealed and artificially aged for 8 h at 160 °C subsequent to the extrusion process (heat treatment T6). Furthermore, stainless steel wires, zinc coated via arc spraying or electro-galvanizing, were employed as reinforcing elements. The standard ram speed was 1 mm/s at an extrusion ratio of 1:10 after the incorporation of the wires and an overall ratio of 1:60. Alternatively, the ram speed was reduced to 0.5 mm/s to investigate its potential influence. The production parameters of the examined profiles are listed in Table 1.

Table 1
Examined specimen states

State	Reinforcing material	Pre-treatment	Heat treatment	Ram speed (mm/s)
S1	Spring steel 1.4310	Initial state	T4	1
S2	Spring steel 1.4310	Ground	T4	1
S3	Spring steel 1.4310	Pickled	T4	1
S4	Spring steel 1.4310	Sandblasted	T4	1
S5	Spring steel 1.4310	Initial state	T4	0.5
S6	Spring steel 1.4310	Initial state	T6	1
S7	Spring steel 1.4310	Zinc coated (arc spraying)	T4	0.5
S8	Spring steel 1.4310	Galvanized with zinc	T4	0.5
C1	Haynes 25	Initial state	T4	1
C2	Haynes 25	Ground	T4	1
N1	Inconel 718	Initial state	T4	1
N2	Inconel 718	Ground	T4	1

2.2. Experimental setup

The stainless steel wires were examined prior to the compound-extrusion using a confocal whitelight microscope (Nanofocus µ-surf) to determine the surface roughness caused by the different pre-treatments.

The push-out specimens were about 1 mm thick. Cutting was done on a precision cut-off machine. The macroscopic size of the reinforcing elements allowed for carrying out push-out-tests on a universal testing machine, which was rebuilt for registering hardness tests using an indenter cone with spherical cap. The specimens were positioned under the axis of the indenter using a light beam and a positioning table prior to being fixed with a downholder. Subsequently, the light pointer was replaced by the indenter and the reinforcing element was pushed out. The match of the light beam with the indenter cap was ensured by appropriate fitting surfaces. Fig. 2 shows the experimental setup and the positioning process using the light pointer. The load–displacement-graphs were registered and the debonding shear strength was subsequently calculated with the maximum load following Eq. (1). The indentation depth was limited to 600 µm since, otherwise, the indenter cone periphery would have touched the matrix material. The results were evaluated sta-

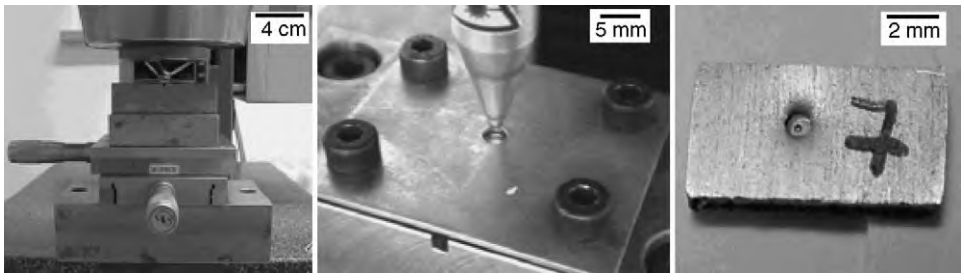

Fig. 2. Experimental setup for the push-out-tests: hardness probe with indenter (left), positioning with a light pointer (centre), specimen with wire pushed out (right).

tistically by calculating Gaussian error distribution curves from the measured values.

Additionally, the manufactured profiles were examined by means of light microscopy. As the compound extrusion process only allows for short-range interfacial diffusion processes and for the formation of intermetallic phases, some samples were prepared for TEM investigations. The samples were prepared from short profile sections by dimpling followed by ion milling in the interfacial region. The sample preparation turned out to be sophisticated as the different metals show significantly different resistance to ion milling. After the push-out-tests, the compounds' interfaces became accessible for visual investigations, which were carried out in the SEM. Both SEM and TEM investigations were accompanied by EDS-analysis.

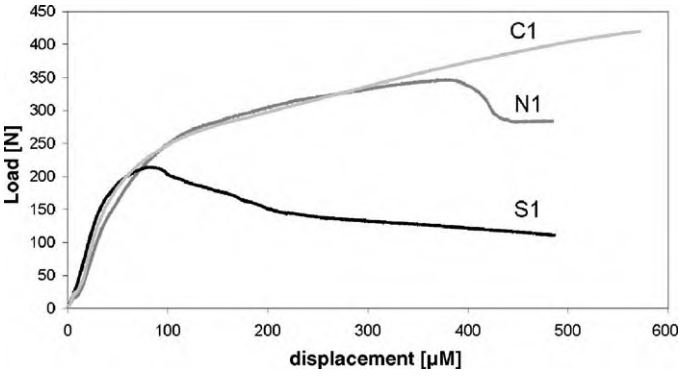

Fig. 3. Load–displacement-curves for specimen states S1, N1, C1 representing the three different measured curve states.

3. Results

3.1. Debonding shear strength

Fig. 3 shows characteristic load–displacement curves for the specimen state S1, C1 and N1, revealing that the initial slope of the curves are nearly identical and that the curve of state C1 increases until the maximum possible penetration depth is reached. The curves of both states N1 and S1 conform to the schematic load–displacement course presented in Fig. 1 comprising the four experimental stages. As a certain penetration of the indenter into the wire is inevitable, the initial slopes slightly decreasing from S1 to N1 indicate small differences in the hardnesses of the different wires investigated due to ultimate tensile strengths of the reinforcements ranging from 2000 to 1400 MPa.

The Gaussian error distribution curves of the debonding shear strengths for the different samples are shown in Fig. 4. Sample state S1 in initial state serves as reference for the debonding shear strength with a value of 61 MPa (see Fig. 4A). The ground state S2 reaches 90 MPa and the pickled one S3 94 MPa representing the highest value of the profiles reinforced with pre-treated stainless spring steel wires. The sandblasted state S4 shows no significant change in debonding strength in comparison to S1 but an increase of scatter. Comparing S1 with S5 and S6 shows

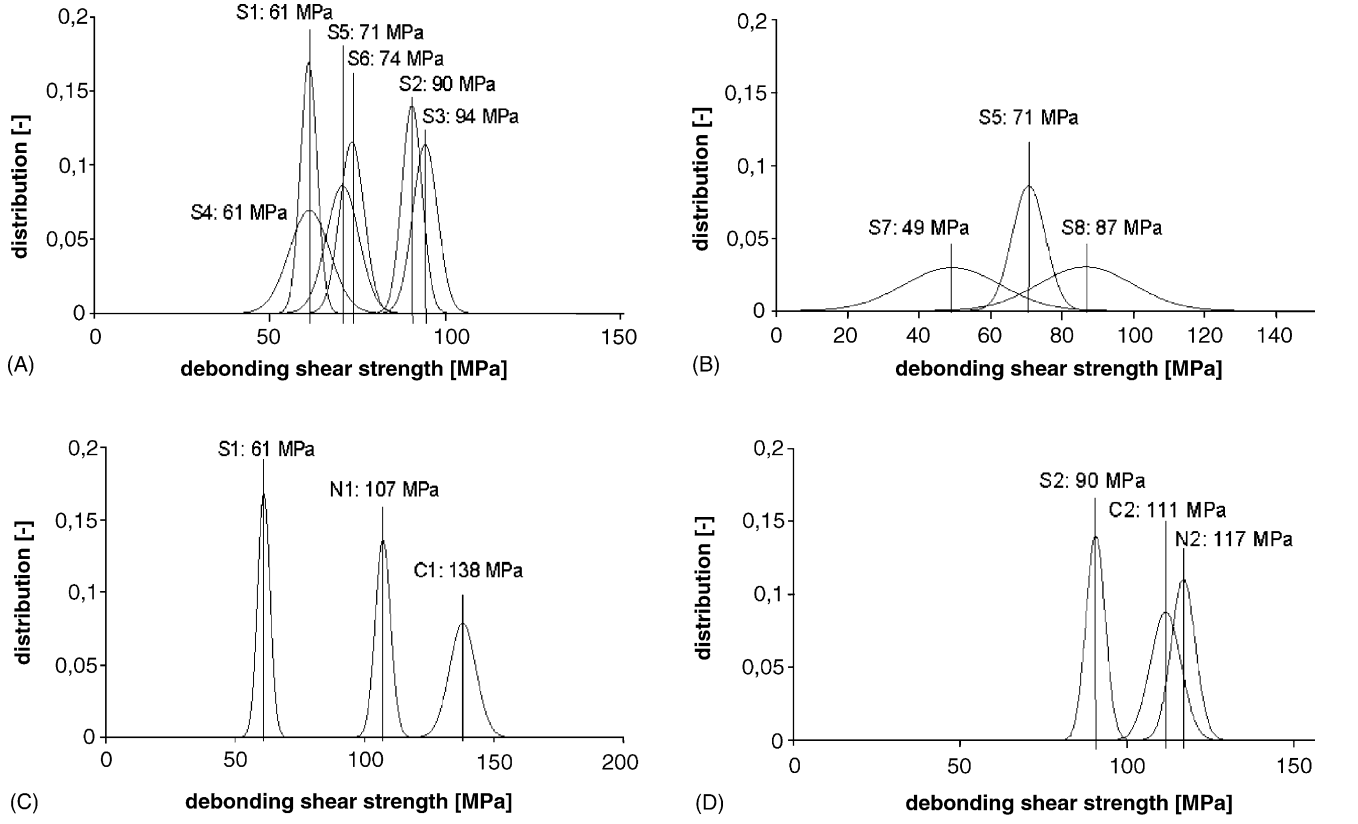

Fig. 4. Mean values and Gaussian error distributions of the debonding shear strength of profiles reinforced with stainless spring steel wires which were subject to different pre- and heat-treatments or were extruded by reduced ram speed (A) and zinc-coated (B). Analogous diagrams for the profiles reinforced with cobalt- or nickel-base alloy wires compared with spring steel reinforced samples (C) or ground wires (D).

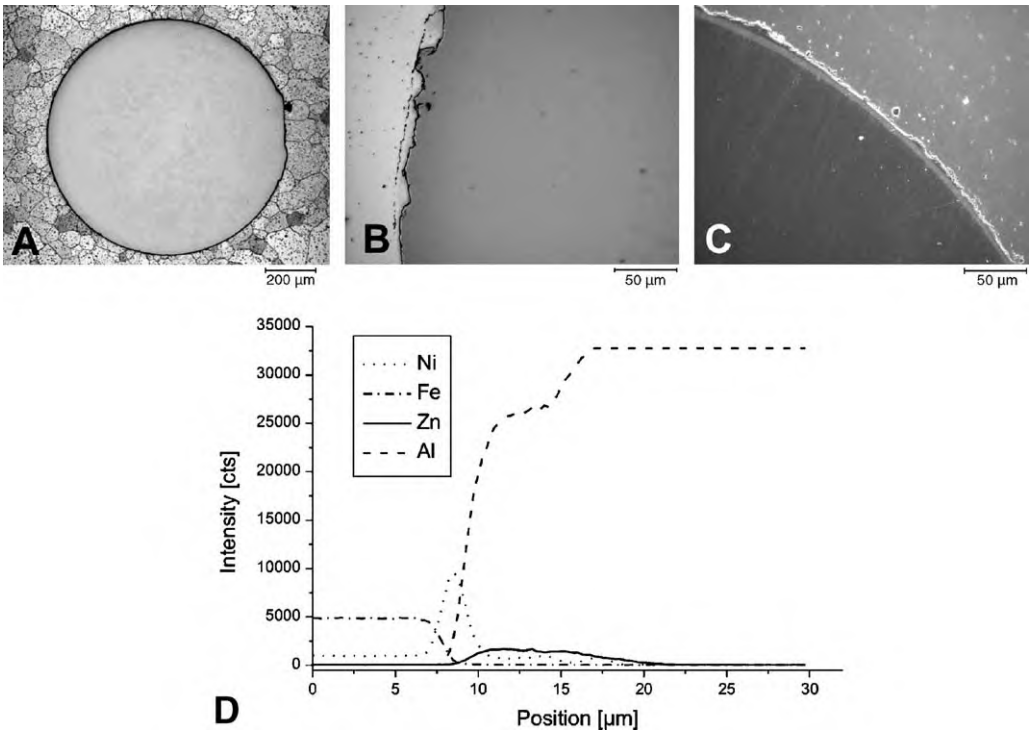

Fig. 5. Micrographs of specimen states S1 (A, initial state, etched with 1% HF), S7 (B, zinc coated by arc spraying) and S8 (zinc coated by electro-galvanizing, C). Microprobe linescan showing the zinc and nickel distribution in S8 (D).

that a subsequent heat-treatment or a reduction of the ram speed increase the debonding shear strength by 20% combined with an incline of the statistical scatter. Due to process requirements, the zinc-coated wires were extruded at a ram speed of 0.5 mm/s and must therefore be compared with S5 (see Fig. 4B). If the coating is applied by arc spraying, the debonding shear strength is reduced by 33% (S7). If the wire is electro-galvanized with zinc (S8), the value is slightly increased when compared to S5. Both coated wire states show a comparably broad statistical scatter. The nickel- or cobalt-base alloy wire reinforced profiles reach both in the initial and in the ground state debonding strength values which are significantly higher than the reference state S1 (see Fig. 4C). For C1 the load increases up to the maximum allowed penetration depth of 600 µm. The value calculated from the measured load at this depth is therefore assumed to represent the minimum debonding shear strength of this state and averages out to 138 MPa. However, the ground wires C2 obtained only 111 MPa. The nickel-base alloy wire reinforced profiles reach 107 MPa in the initial state N1 and 117 MPa when ground (see Fig. 4D). These results reveal an overall increase of 75 up to 125% in comparison to the stainless steel reference state.

3.2. *Metallographic investigations*

Micrographs of specimens S7 and S8 are shown in Fig. 5 in comparison to the reference state S1. Even higher resolutions reveal no gap between the matrix material and the reinforcement. The coated reinforcing elements in specimen state S7 and S8 are surrounded by an interface containing zinc. In state S7, the interface has circumferential cracks. In S8, the micrographs reveal a two-layer interface resulting from the electro-galvanizing with an inner layer of nickel and an outer, partially degenerated layer of zinc. This result is confirmed by microprobe analysis. As diffusion processes are localised on nanome-

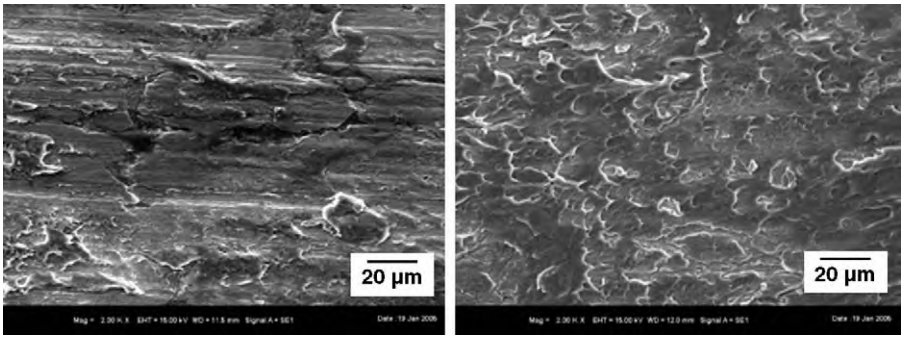

Fig. 6. SEM micrographs of the wire–matrix interface of specimen state S1 (left) and S3 (right) after push out.

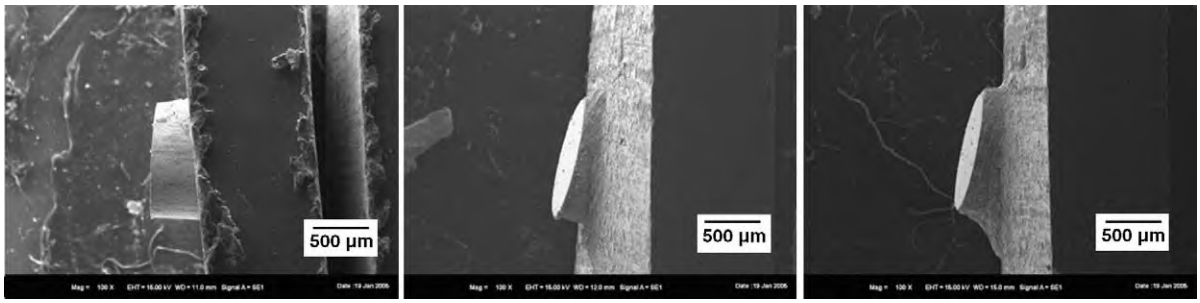

Fig. 7. SEM micrographs (side view) of specimen states S1 (left), N1 (centre) and C1 (right) after push-out-tests. N1 and C1 show severe plastic deformation of the matrix in comparison to S1.

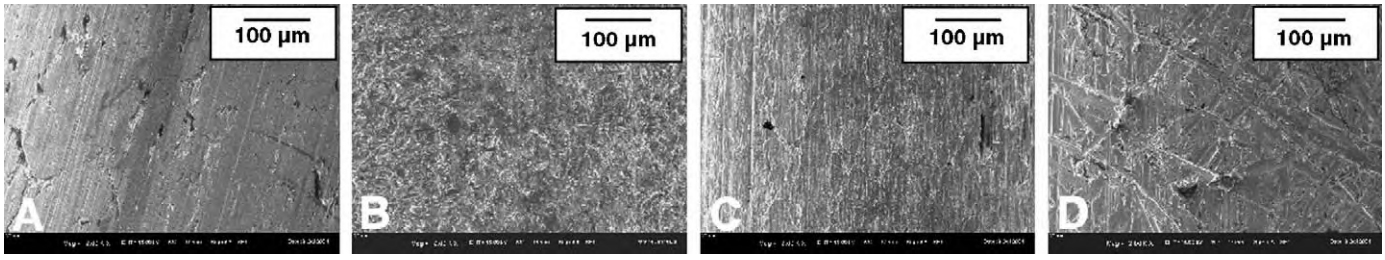

Fig. 8. SEM micrographs (magnification 2000×) of pre-treated stainless steel wires in comparison to the initial state (A), sandblasted (B), pickled (C) and ground (D).

tre scale, the uncoated specimens reveal no distinct interfacial zone and/or intermetallic phases at the interface applying light-microscopy.

SEM micrographs of pushed out specimens reveal aluminium remaining on the reinforcement surfaces and indicate that debonding takes place partially inside the matrix. Accordingly the fractured surface exhibits a dimple morphology suggesting a ductile fracture. Fig. 6 shows that the reinforcement surface of specimen state S3, which has the highest debonding shear strength of the spring steel reinforced profiles, is completely covered by aluminium, while in S1 the original wire surface is clearly visible. The fracture morphology of the nickel-base or cobalt-base alloy wire reinforced specimens is comparable to S3. Some regions of the fractured surfaces of S7 and S8 contain zinc—for S8 also nickel—indicating that the fracture propagated partially inside the applied coatings. Fig. 7 presents the push-out morphology of specimen states N1 and C1 in comparison to S1. The significantly higher debonding shear strength leads to plastic deformation of the matrix surrounding the wire. This effect is also indicated by the corresponding load–displacement-curves with an extended stage 2 for specimen state N1 and C1 (see Fig. 3).

Table 2
Roughness along the wire axis of the pre-treated stainless steel wires

Wire material	Pre-treatment	Roughness Ra [µm]	Incorporated in specimen state
Spring steel 1.4310	Initial state	0.114	S1 (S5, S6)
Spring steel 1.4310	Sandblasted	0.346	S4
Spring steel 1.4310	Pickled	0.540	S3
Spring steel 1.4310	Ground	0.725	S2

3.3. Topography of the reinforcing elements

Fig. 8 shows SEM micrographs of pre-treated stainless spring steel wires in comparison to the referende state S1. Roughness measurements with whitelight microscopy show that pickled or ground wires possess the highest mean surface roughness value (Ra) in comparison to the initial state. The difference in Ra indicates the activation of the wire surface prior to embedding in the aluminium matrix due to an increase of the specific wire surface and/or an ablation of the passivating chrome oxide layer. Table 2 summarizes the measured roughness values Ra.

3.4. TEM investigations

The short-time thermal impact during the extrusion process only allows for local diffusion processes on the nanometre scale. Therefore, investigations on diffusion zones or the formation of intermetallic phases near the wire–matrix-interface have to be carried out by transmission electron microscopy. Interdiffusion of elements was detected by EDS line-scans perpendicular to the interface. For all material combinations the existence of near-interface intermetallics inside the matrix containing wire elements could be proved. For the system AA6060-stainless steel, the intermetallic phases were identified as iron aluminide (Al_5Fe_2) containing some chromium. The intermetallics in the nickel- or cobalt-base alloy reinforced profiles formed agglomerates of small grains. Hereby, the size of the intermetallics allowed neither for analyzing the composition of the individual grains nor for recording a diffraction pattern. Fig. 9 presents TEM micrographs of the detected near-interface intermetallic phases.

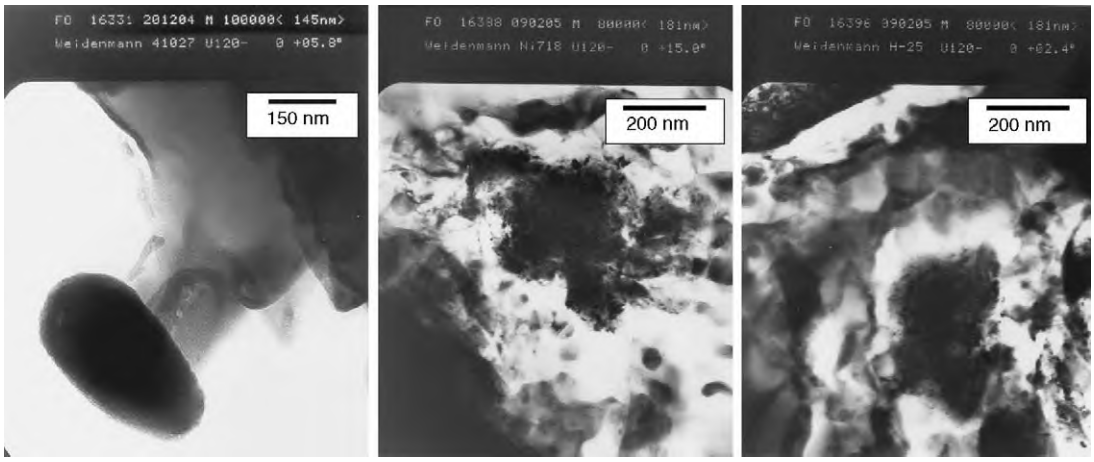

Fig. 9. TEM micrographs of near-interface intermetallic precipitations: Al_5Fe_2 (left) in the system 6060 + 1.4310; agglomerates of intermetallics containing nickel or cobalt and chromium in the system 6060 + Inconel 718 (centre) or 6060 + Haynes 25 (right).

Additionally, the EDS line-scans perpendicular to the interface showed that the heavy metals iron, chromium, nickel and cobalt tend to diffuse into the matrix material having the higher homologous temperature during the extrusion process. The width of the diffusion zone ranges from 50 up to 500 nm. The diffusion of aluminium into the wire could not be detected for any of the combinations investigated.

4. Discussion

Provided that typical shear strengths of aluminium wrought alloys are within 65% and 75% of the ultimate tensile strength—typically 160 MPa for AA6060 in state T4 [8], the maximum shear strength of the pure matrix material is about 120 MPa. The push-out-tests have shown that various parameters influence the debonding shear strength in compound extruded profiles. Starting from 61 MPa for the initial state the debonding shear strength increases by 50% for ground and pickled stainless steel wires, while sand blasting has no effect on the debonding strength. The significantly lower increase of the surface roughness Ra for sandblasted wires in comparison to ground or pickled ones indicates that the surface chromium oxide layer is not ablated, as it is the case for pickled or ground wires, but just roughened. Only the last mentioned pre-treatments activate the surface sufficiently. Consequently, the failure of the interface relocates into the matrix, which is proven by SEM investigations (Fig. 6). Changing the reinforcing materials to nickel- or cobalt-base alloy additionally increases the debonding shear strength to a maximum value of 138 MPa, combined with a prominent plastic deformation of the matrix surrounding the reinforcing wire as indicated by the morphology of the corresponding load–displacement-curves and the SEM micrographs after the push-out-tests (see Fig. 9). The metallurgical bond between wire and matrix is based on diffusion of heavy elements like nickel, cobalt, iron or chromium into the aluminium matrix and the formation of near-interface intermetallic phases, respectively. For stainless spring steel wire reinforced specimens, the detected intermetallic phase is Al_5Fe_2 additionally containing chromium, which was already found by [2]. More than this comparably brittle intermetallic phase, the intermetallic phases in cobalt- and nickel-containing systems increase the debonding shear strength up to 138 MPa—a value, that even exceeds the expected maximum shear strength of pure AA6060. Zinc layers are only suitable to a limited extent. Arc-sprayed zinc layers feature pores leading to the formation of circular cracks drastically decreasing the debonding shear strength. Electro-galvanized wires with a nickel-strike intermediate layer perform better, partially leading to the formation of nickel- and aluminium-containing near-interface regions. Therefore, the debonding shear strength is increased. However, the inhomogeneous zinc distribution, which was detected by microprobe analysis, causes an increased statistical spread of the measured debonding shear strengths. An additional artificial ageing (T6) or a reduction of the ram speed ameliorate the debonding shear strength. For the last-mentioned procedure, this effect is caused by an extended retention period at extrusion temperature facilitating diffusion processes.

5. Summary and conclusions

The push-out-technique is an adequate method for measuring the debonding shear strength in macroscopic compounds. Pre-treatments may enhance the debonding shear strength, if they activate the wire surface significantly. Grinding and pickling increase the shear strength for stainless steel wires. Nickel-base alloy wires perform better when ground, while cobalt-base wires should remain in the initial state. The use of nickel- or cobalt-base alloy wires increases the debonding shear strength and even slightly exceeds the expected maximum level due to the formation of strength-increasing intermetallic precipitates. The brittle iron aluminide particles evolving in stainless steel reinforced aluminium matrix compounds lead to a comparably weak interface.

An additional heat treatment (T6) or a reduction of the ram speed improves the debonding shear strength.

Zinc coatings achieve better results when they are electro-galvanized as they are defect-free and feature a strength-increasing nickel intermediate layer.

Acknowledgements

This paper is based on investigations of the Transregional Collaborative Research Centre SFB/TR10, which is kindly supported by the German Research Foundation (DFG).

References

[1] A. Klaus, M. Schomäcker, M. Kleiner, Light Metal Age 62 (8) (2004) 12–21.
[2] A. Wagner, U. Hodel, Konf.-Einzelbericht: Neue Verfahren der Massivumformung, Symp. d. DGM, Bad Nauheim, 1983, pp. 177–195.
[3] D.B. Marshall, J. Am. Ceram. Soc. 67 (1984) C259–C260.
[4] T.W. Clyne, P.J. Withers, An Introduction to Metal Matrix Composites, Cambridge University Press, Cambridge, Groβbritannien, 1993.
[5] J. Janczak, R. Stackpole, G. Bürki, L. Rohr, Proceedings of the 17th International Conference on SAMPE, Basel, Schweiz, 1996.
[6] J. Janczak, L. Rohr, P. Schulz, H.P. Degischer, Oberflächen Werkstoffe 36 (1995) 16–19.
[7] T.P.D. Rajan, R.M. Pillai, B.C. Pai, J. Mater. Sci. 33 (1998) 3401–3503.
[8] F. Ostermann, Anwendungstechnologie Aluminium, Springer-Verlag, Berlin, 1998.